



# Zinc oxide nanoparticles cooperate with the phyllosphere to promote grain yield and nutritional quality of rice under heatwave stress

Shuqing Guo<sup>a</sup> , Xiangang Hu<sup>a,1</sup> , Zixuan Wang<sup>a</sup>, Fubo Yu<sup>a</sup>, Xuan Hou<sup>a</sup>, and Baoshan Xing<sup>b</sup>

Affiliations are included on p. 10.

Edited by Catherine Murphy, University of Illinois at Urbana-Champaign, Urbana, IL; received July 25, 2024; accepted September 19, 2024

To address rising global food demand, the development of sustainable technologies to increase productivity is urgently needed. This study revealed that foliar application of zinc oxide nanoparticles (ZnO NPs; 30 to 80 nm, 0.67 mg/d per plant, 6 d) to rice leaves under heatwave (HW) stress increased the grain yield and nutritional quality. Compared with the HW control, the HWs+ZnO group presented increases in the grain yield, grain protein content, and amino acid content of 22.1%, 11.8%, and 77.5%, respectively. Nanoscale ZnO aggregated on the leaf surface and interacted with leaf surface molecules. Compared with that at ambient temperature, HW treatment increased the dissolution of ZnO NPs on the leaf surface by 25.9% and facilitated their translocation to mesophyll cells. The Zn in the leaves existed as both ionic Zn and particulate ZnO. Compared with the HW control, foliar application of ZnO NPs under HW conditions increased leaf nutrient levels (Zn, Mn, Cu, Fe, and Mg) by 15.8 to 416.9%, the chlorophyll content by 22.2 to 24.8%, Rubisco enzyme activity by 21.2%, and antioxidant activity by 26.7 to 31.2%. Transcriptomic analyses revealed that ZnO NPs reversed HW-induced transcriptomic dysregulation, thereby enhancing leaf photosynthesis by 74.4%. Additionally, ZnO NPs increased the diversity, stability, and enrichment of beneficial microbial taxa and protected the phyllosphere microbial community from HW damage. This work elucidates how NPs interact with the phyllosphere, highlighting the potential of NPs to promote sustainable agriculture, especially under extreme climate events (e.g., HWs).

nanotechnology | food safety | sustainable agriculture | heatwaves | phyllosphere microbial community

The global population is projected to reach approximately 10 billion by 2050 and lead to a surge in food demand, which is estimated to increase by 35 to 56% from 2010 to 2050 (1, 2). Such an increase in demand poses a significant challenge in terms of providing quality food to meet the needs of the expanding populace. The primary method used to increase crop yields is the application of conventional fertilizers. However, the low use efficiency of conventional fertilizers (for example, only 30 to 35% of the applied nitrogen, 35 to 40% of the applied potassium fertilizers, and 18 to 20% of the applied phosphorus are taken up by plants) has resulted in their overapplication, which has caused significant environmental damage, such as water pollution (e.g., eutrophication), soil acidification, biodiversity loss, and climate change (3, 4). It is estimated that emissions from conventional fertilizers contribute to 14 to 18% of the total greenhouse gas emissions worldwide, which is nearly half that of the current contribution due to food production (5). In particular, the application of nitrogen fertilizers during agricultural production alone results in the release of 245 to 308 million metric tons of CO<sub>2</sub> equivalent emissions annually (6). Climate change, driven by greenhouse gas emissions, is expected to exacerbate food insecurity (7). Therefore, addressing the increasing global food demand necessitates the development of sustainable technologies that can replace conventional fertilizers and increase productivity in the context of climate change.

Owing to climate change, the global frequency of weather extremes, such as heatwaves (HWs), is increasing, which negatively impacts agricultural production and food security (8, 9). The World Meteorological Organization Commission for Climatology defined a HW as an extended period of exceptionally high temperatures lasting a minimum of two consecutive days during the warm season that surpasses the predetermined thresholds according to regional climate norms (10). In accordance with the standards set by the China Meteorological Administration, HWs are defined as periods in which the daily maximum temperature exceeds 35 °C for at least three consecutive days (11). Nanotechnology has been recognized as a technological breakthrough that can improve stress tolerance in plants and

## Significance

Nanotechnology has shown promise in addressing the growing global food demand from the increasing global population. However, full life cycle experiments addressing the agricultural feasibility of nanotechnology in extreme climate events, such as heatwaves (HWs), are lacking. Here, we demonstrate that foliar application of zinc oxide nanoparticles (ZnO NPs) significantly increases the grain yield and nutritional quality of rice during HWs. Multiomics analysis revealed that the ZnO NPs facilitated nutrient uptake and photosynthesis under HW conditions via physiological regulation and restructuring of the phyllosphere microbial community. This study advances the understanding of NP–phyllosphere interactions and validates the agricultural applicability of nanotechnology for mitigating the impacts of extreme climate events.

Author contributions: X. Hu designed research; S.G. performed research; X. Hu contributed new reagents/analytic tools; S.G., Z.W., F.Y., X. Hou, and B.X. analyzed data; and S.G. and X. Hu wrote the paper.

The authors declare no competing interest.

This article is a PNAS Direct Submission.

Copyright © 2024 the Author(s). Published by PNAS. This article is distributed under Creative Commons Attribution-NonCommercial-NoDerivatives License 4.0 (CC BY-NC-ND).

<sup>1</sup>To whom correspondence may be addressed. Email: huixiangg@nankai.edu.cn.

This article contains supporting information online at <https://www.pnas.org/lookup/suppl/doi:10.1073/pnas.2414822121/-DCSupplemental>.

Published November 4, 2024.

increase agricultural productivity (12–14). A field study revealed that iron oxide nanoparticles (10 mg/kg soil) decreased greenhouse gas emissions in paddy soil and significantly improved rice yields by 23.6 to 54.9% (15). However, field studies are limited, and most studies have been conducted using pot experiments. Foliar application of 400 mg/L silica NPs stimulated the synthesis of antioxidant enzymes and chlorophyll, leading to a 58.6% increase in groundnut yield (16). In soybean grains under drought stress, carbon dots (5 mg/kg soil) increased the protein, fatty acid, and amino acid contents by 3.4%, 6.9%, and 17.3%, respectively, by increasing nitrogen bioavailability (13). Compared with conventional agrochemicals, NPs offer controllable nutrient release to crops, superior plant growth promotion, heightened utilization efficiency, and fewer negative environmental impacts (17, 18). Thus, NPs have shown promise to more effectively increase the productivity of crops under environmental stress compared with traditional agrochemicals (19).

Zinc (Zn) is an essential micronutrient that is crucial for plant growth and contributes to vital physiological processes in plants, such as photosynthesis, chlorophyll and enzyme biosynthesis, and stress mitigation (17). However, global soil Zn deficiency poses a significant ecological concern and negatively affects crop yield and quality (18, 20). Moreover, Zn deficiency is one of the most pervasive nutritional deficiencies worldwide, affecting one-third of the human population (21). Zn, when applied as a fertilizer during crop growth, enhances both productivity and the Zn content in the edible parts of the plant, which ensures adequate human uptake from the food (22). Foliar Zn application prevents large amounts of Zn being lost and is considered a more efficient method than soil Zn application (18). However, the Zn salts (e.g.,  $\text{ZnSO}_4$  and  $\text{ZnCl}_2$ ) used in foliar fertilizers exhibit low Zn utilization efficiency and may cause adverse effects such as leaf scorching (23). Zinc oxide nanoparticles ( $\text{ZnO}$  NPs), an alternative foliar Zn fertilizer, can be absorbed by the leaves through the stomata and accumulate within mesophyll tissue for effective and sustained  $\text{Zn}^{2+}$  delivery (24). Notably, foliar application of  $\text{ZnO}$  NPs (15 mg/L) increased pumpkin biomass by 33.3% (25). Similarly, a relatively high concentration of  $\text{ZnO}$  NPs (50 mg/L) improved the nutritional quality of tomato fruits, increasing the total phenolic compound content by 25.7%, the amino acid content by 22.9%, and the Zn content by 42.0% (26). Additionally, foliar application of  $\text{ZnO}$  NPs (90 mg/L) to alfalfa seedlings under heat stress increased the plant biomass by 29.7 to 45.5% and mitigated heat-induced damage to chloroplasts, mitochondria, and cell walls, indicating the potential of using  $\text{ZnO}$  NPs to enhance crop growth under heat stress (27). However, studies on NP–phyllosphere interactions and the full life cycle of the agricultural feasibility of using  $\text{ZnO}$  NPs during HWs are still lacking.

The aboveground section of a plant that hosts a diverse array of microbes is known as the phyllosphere (28). Phyllosphere-colonizing microorganisms are crucial for leaf function, overall plant health, crop yield, and agricultural sustainability (29). However, prior investigations on the impacts of climate change and NP application have focused primarily on the soil and rhizosphere (30). Moreover, studies have revealed that  $\text{ZnO}$  NPs can benefit soil bacterial communities, including enriching the beneficial endophytic and rhizosphere microorganisms and increasing soil microbial richness and diversity (31, 32). However, whether  $\text{ZnO}$  NPs have similar positive effects on the phyllosphere microbial community has not been explored. Climate change, particularly heat stress, can disrupt the stability of phyllosphere microbial communities, potentially reducing the abundance of beneficial species and favoring pathogens (30). Therefore, we hypothesize that foliar application of  $\text{ZnO}$  NPs may preserve the stability of phyllosphere microorganisms under HW conditions.

Rice is the main staple food for more than half of the world's population, with its production covering millions of hectares worldwide, and serves as a valuable model for assessing plant responses to NPs (15, 33, 34). We investigated the foliar uptake, dissolution, and translocation of nanoscale  $\text{ZnO}$  and its interactions with the phyllosphere during HWs. We hypothesized that  $\text{ZnO}$  NPs release  $\text{Zn}^{2+}$  ions on leaves, thereby influencing the physiological metabolism in the foliage. The yield and nutritional quality of the rice grains were also assessed. Moreover, comprehensive multiomics analyses (metabolomics, transcriptomics, and microbiomics), as well as assessments of physiological and biochemical parameters, such as Zn content and distribution, photosynthetic efficiency, macro- and micronutrient levels, and antioxidant enzyme activities, were conducted to elucidate the multiple functions of  $\text{ZnO}$  NPs on leaves during HWs. These findings highlight the potential of  $\text{ZnO}$  NPs as efficacious micronutrient fertilizers capable of sustainably increasing crop productivity during extreme climate events.

## Results and Discussion

### **$\text{ZnO}$ NPs Increased Grain Yield and Nutritional Quality during HWs.**

Compared with  $\text{ZnO}$  NPs,  $\text{Zn}^{2+}$  ions more strongly increased the leaf Zn content (Fig. 1A), indicating that Zn delivery via Zn ions ( $\text{ZnSO}_4$ ) was more effective than that via  $\text{ZnO}$  NPs. Moreover, HWs significantly decreased the leaf starch content and shoot biomass (Fig. 1B and C); however, compared with  $\text{Zn}^{2+}$  ions,  $\text{ZnO}$  NPs stably and significantly improved plant growth and starch content, especially during HWs (Fig. 1B and C). Fertilizers with soluble forms of Zn (e.g.,  $\text{ZnSO}_4$ ) tend to rapidly release substantial quantities of  $\text{Zn}^{2+}$  ions, which readily complex with phytate within the leaf, limiting Zn mobility and availability in the plant and potentially resulting in low utilization efficiency or phytotoxicity to crops (18).  $\text{ZnO}$  NPs sustain the release of Zn into plants, thereby meeting the dynamic spatiotemporal nutritional requirements of crops (35). Consequently, compared with  $\text{Zn}^{2+}$  ions,  $\text{ZnO}$  NPs promoted rice growth more effectively at both ambient temperature and under HW conditions. In addition, nanostructures exhibit better retention on leaves than do metal salts or chelated metal ions because of their strong adhesion, leading to increased bioavailability, reduced runoff, and a lower environmental impact (36). Foliar-sprayed  $\text{ZnO}$  NPs can reach the surrounding soil after being washed away by rain, potentially affecting the plants and rhizosphere (e.g., microbes and soil enzymes). However, in fields subjected to prolonged (3 y) and repeated (three times) applications of  $\text{ZnO}$  NPs (10 mg/kg soil), significant changes in plant health and the soil microbial community structure were not observed, suggesting that  $\text{ZnO}$  NPs could serve as effective, sustainable, and environmentally friendly materials (37).

Compared with soluble Zn fertilizers,  $\text{ZnO}$  NPs better enhanced rice seedling growth during HWs. To assess the potential of using  $\text{ZnO}$  NPs to improve agricultural production during HW days, rice plants at the flowering stage were subjected to daily foliar application of  $\text{ZnO}$  NPs, followed by HW treatment; coexposure lasted for 6 d (Fig. 1D). Under HW conditions, the  $\text{ZnO}$  NPs significantly increased the grain Zn content by 21.6% (Fig. 1E). Zn is an essential nutrient for plant and human health (38), and such a significant increase in Zn content in grain resulting from foliar application of  $\text{ZnO}$  NPs could facilitate the intake of adequate Zn via the daily human diet. The application of  $\text{ZnO}$  NPs led to a 23.7% increase in grain weight under ambient temperature conditions and a 22.1% increase under

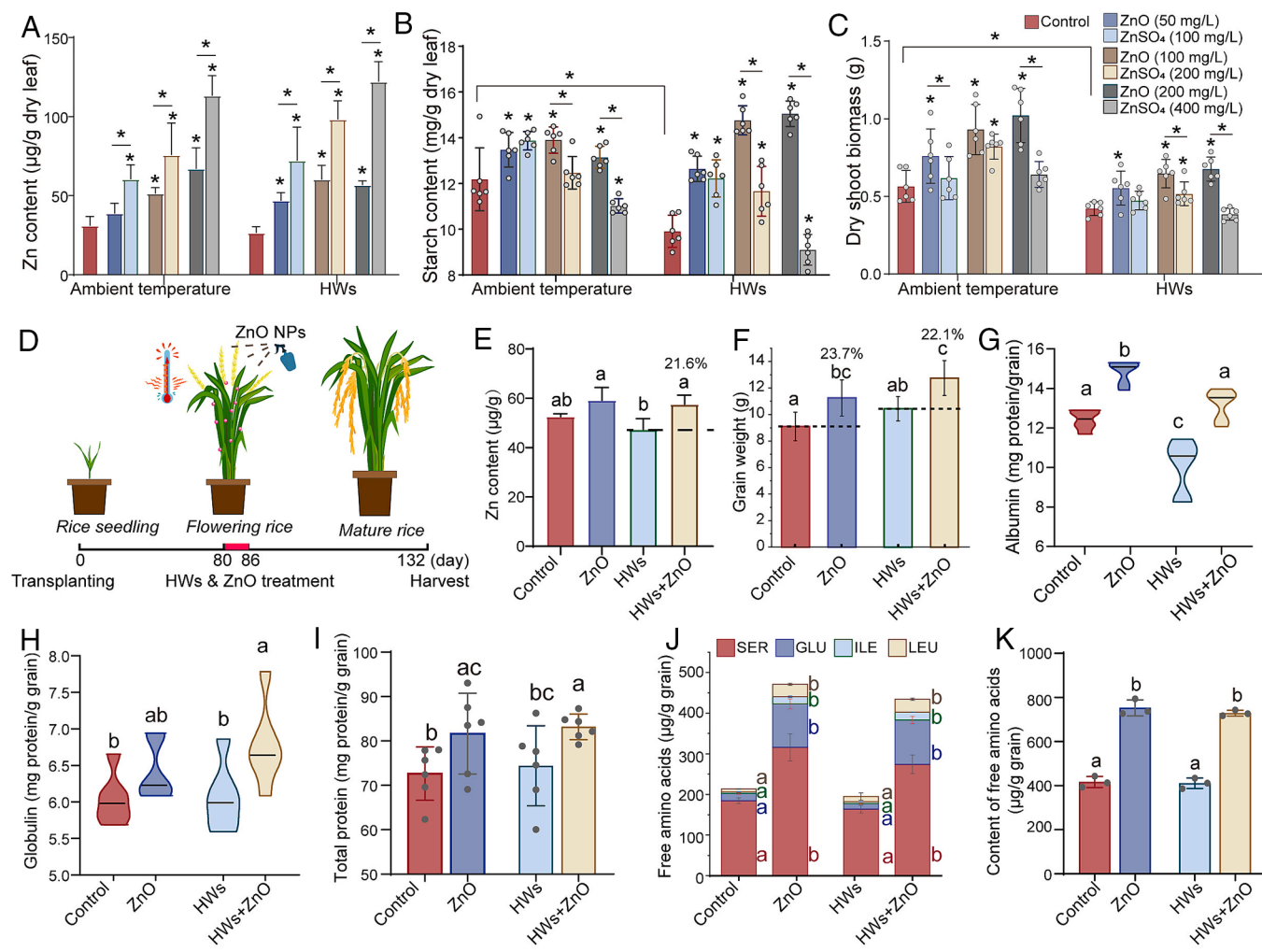


**Fig. 1.** Biomass and rice production in response to HWs, Zn<sup>2+</sup> ions, and ZnO NPs. (A–C) Zn content in, starch content in and dry shoot biomass of rice seedlings treated with ZnO NPs (50, 100, and 200 mg/L) or the equivalent concentration of Zn<sup>2+</sup> ions (100, 200, and 400 mg/L ZnSO<sub>4</sub>) at ambient temperature or under HW conditions. (D) Schematic of the design of the full life cycle experiment. (E) Zn content in the grain. (F) Grain weight per plant. (G) Albumin. (H) Globulin. (I) Total soluble protein in the grain. (J) Variations in free amino acids. SER: serine; GLU: glutamic acid; ILE: isoleucine; LEU: leucine. (K) Total free amino acid content in the grain. The data are presented as the means of three (A, E, J, and K) or six (B and C and F–I) replicates ± the SD. Asterisks and different lowercase letters denote a statistically significant difference based on LSD pairwise comparisons ( $P < 0.05$ ).

HW conditions (Fig. 1F). Notably, HWs did not significantly reduce rice yield. Previous studies have shown that the decrease in grain production during HWs was primarily due to drought accompanying the HW (39), which can be mitigated by supplying sufficient water for rice growth. HWs resulted in a significant 19.3% reduction in the albumin concentration, whereas ZnO NPs increased the albumin concentration by 19.6% under ambient temperature conditions and by 32.1% under HW conditions (Fig. 1G). Additionally, ZnO NPs increased the globulin content by 6.3% and 11.7% and increased the total soluble protein content by 12.4% and 11.8% at ambient temperature and under HW conditions, respectively (Fig. 1H and I). The contents of glutelin and prolamin were not significantly increased by ZnO NPs under HW conditions (SI Appendix, Fig. S1). ZnO NPs significantly elevated the levels of serine, glutamic acid, isoleucine, and leucine in grains at both ambient temperature and under HW conditions (Fig. 1J). The application of ZnO NPs resulted in increases in total free amino acids of 80.7% and 77.5% at ambient temperature and under HW conditions, respectively (Fig. 1K). Thus, ZnO NPs can effectively increase rice yield and enrich grain nutrients when considering climate change and global food shortages.

**HWs Increased Dissolution of the ZnO NPs on the Leaf Surface.** ZnO NPs are notably present near the stomata, indicating a possible route for their entry into leaf tissue (SI Appendix, Fig. S2). ZnO NPs aggregated on the leaf surface at both ambient temperature and under HW conditions, with the observed aggregate sizes ranging from 1 µm to several hundred microns (Fig. 2A). At both ambient temperature and under HW conditions, many ZnO NPs were distributed around large silica bodies, some of which adhered to the silica bodies and trichome hairs (Fig. 2A and SI Appendix, Figs. S3 and S4). The tendency of these NPs to aggregate on the leaves could be attributed to van der Waals interactions (40). Upon energy-dispersive spectroscopy (EDS) analysis, the ZnO aggregates presented multiple signals, including those from carbon (C), oxygen (O), Zn, and silicon (Si), under both ambient and HW conditions (Fig. 2A). Before entering plants, NPs can interact with surrounding molecules to form dynamic layers with biomolecules (e.g., peptides, lipids, and plant secretions), a phenomenon termed the eco-corona (41). The multiple signals from the ZnO NPs can be attributed to the formation of an eco-corona on the NP surface (interactions between the NPs and the leaf cuticle or secretions) (40). A total of 132 metabolites on the leaf surface were identified and semiquantified (SI Appendix, Fig. S5) and

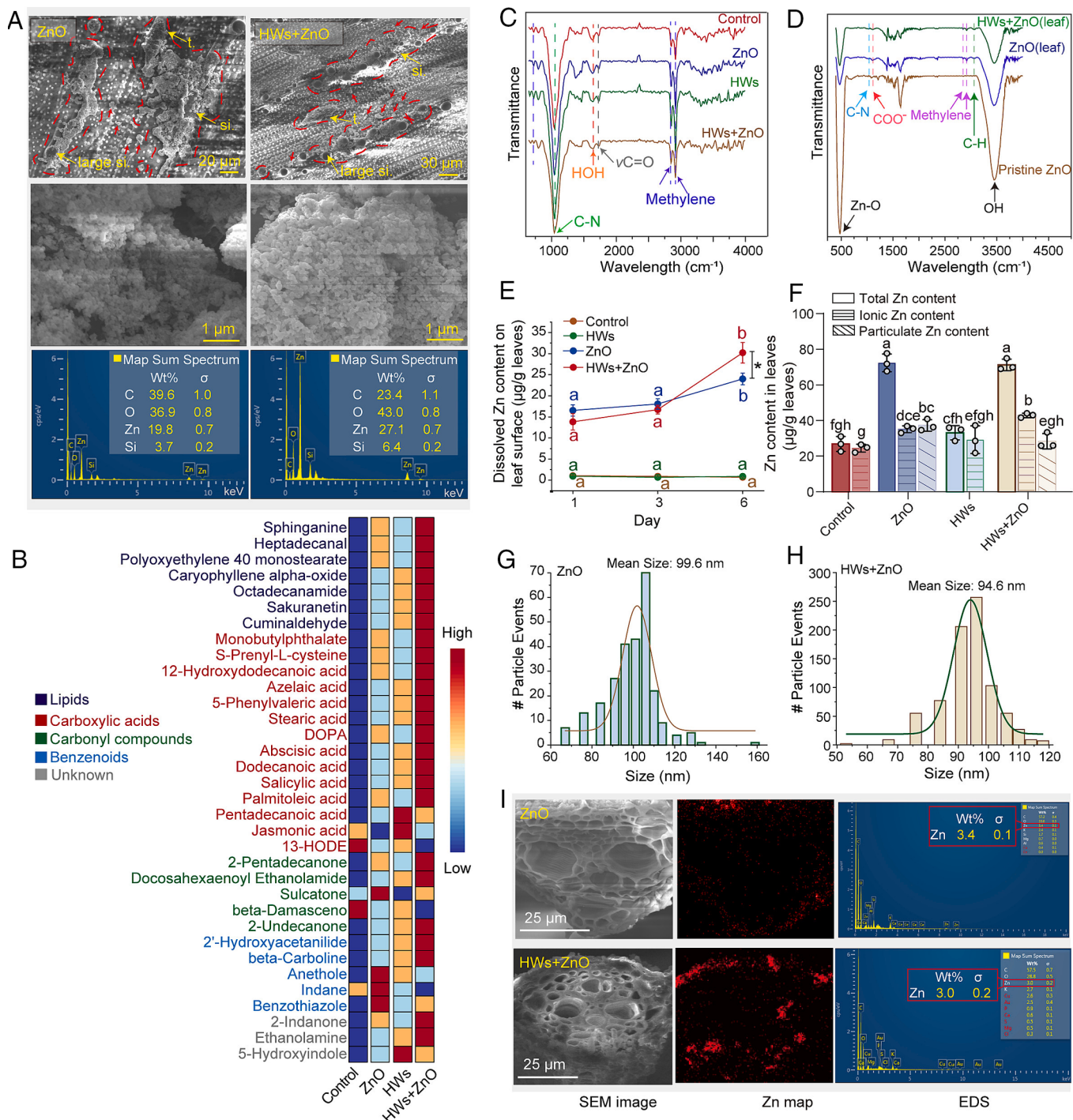


**Fig. 2.** Dissolution of ZnO NPs on the leaf surface and within the leaves. (A) Scanning electron microscopy (SEM) images and EDS analysis of ZnO aggregates on the leaf surface. The red circles and arrows indicate ZnO aggregates on the leaf surface. t., trichome hairs; si., silica bodies; large si., large silica bodies. (B) Heatmap of leaf surface metabolites identified via PLS-DA with variable importance in projection (VIP) scores  $\geq 1.2$ . (C) ATR spectral features of rice leaves. (D) Fourier transform infrared (FTIR) spectra of pristine ZnO NPs and ZnO NPs on the leaf surface. (E) Dissolved Zn content on the leaf surface. (F) Total, dissolved, and particulate Zn contents within rice leaves. Particle size distribution of the NPs within the leaves in the (G) ZnO group and (H) HWs+ZnO group. (I) SEM images and EDS analysis of rice leaves sprayed with ZnO NPs under ambient temperature conditions and HWs. The data are presented as the means of three (E and F)  $\pm$  the SD. Asterisks and different lowercase letters denote a statistically significant difference based on LSD pairwise comparisons ( $P < 0.05$ ).

were primarily categorized as lipids (38.6%), benzenoids (13.6%), peptides (12.1%), and organic acids (6.8%) (SI Appendix, Fig. S6). Principal component analysis (PCA) revealed that the ZnO, HWs, and HWs+ZnO treatments induced changes in the leaf surface metabolite profile (SI Appendix, Fig. S7). Partial least squares discriminant analysis (PLS-DA) identified 34 features, predominantly lipids, carboxylic acids, carbonyl compounds, and benzenoids (Fig. 2B). Compared with those in the control group,

almost all the identified metabolites were upregulated in response to the ZnO, HWs, and HWs+ZnO treatment (Fig. 2B).

The attenuated total reflectance (ATR) spectra of the rice leaves revealed features at  $725\text{ cm}^{-1}$ ,  $2,846\text{ cm}^{-1}$ , and  $2,916\text{ cm}^{-1}$  (Fig. 2C), which were assigned to the stretching and rocking doublets of methylene ( $\text{CH}_2$ ) in alkanes (42). The signals at  $1,041\text{ cm}^{-1}$  and  $1,635\text{ cm}^{-1}$  corresponded to C–N stretching in peptides and HOH bending, respectively (Fig. 2C) (42, 43). The ester carbonyl stretching feature

at  $1,728\text{ cm}^{-1}$  was likely caused by cutin (Fig. 2C) (42). The ZnO aggregates on the leaf surface and pristine ZnO NPs presented similar features at  $474\text{ cm}^{-1}$  and  $3,448\text{ cm}^{-1}$ , which were attributed to Zn—O stretching and OH stretching, respectively (Fig. 2D) (44). However, the features at  $1,039\text{ cm}^{-1}$  (C—N stretching),  $1,107\text{ cm}^{-1}$  (carboxyl symmetrical stretching),  $2,850\text{ cm}^{-1}$  ( $\text{CH}_2$  stretching),  $2,916\text{ cm}^{-1}$  ( $\text{CH}_2$  stretching), and  $3,066\text{ cm}^{-1}$  (aromatic groups with C—H stretching) (45) were detected only in the sample of ZnO aggregates on the leaf surface (Fig. 2D). These results suggest that NP aggregates on the leaf surface interact with leaf surface molecules to form an eco-corona comprising alkanes ( $\text{CH}_2$ ), benzenoids (aromatic groups with C—H stretching), peptides (C—N), and carboxylic acids (carboxyl).

The foliar application of ZnO NPs significantly increased the contents of both total Zn and ionic Zn on the leaf surface, indicating the deposition and subsequent dissolution of the ZnO NPs (Fig. 2E and *SI Appendix*, Fig. S8). There were no significant differences in ZnO NP deposition between the ZnO and HWs+ZnO treatment groups ( $P > 0.05$ ; *SI Appendix*, Fig. S8). This finding aligns with the leaf wettability and roughness results (*SI Appendix*, Figs. S9 and S10), which primarily influence NP retention on leaves (36). However, compared with that in the ZnO group, the ionic Zn content on the leaf surface in the HWs+ZnO group increased by 25.9% ( $P < 0.05$ , Fig. 2E). The dissolution of ZnO NPs in Milli-Q (MQ) water revealed that short-term (6 d) HW treatment did not affect NP dissolution (*SI Appendix*, Fig. S11). Therefore, the interactions between the leaf surface molecules and NPs (Fig. 2D) may influence the subsequent dissolution processes (40). Previous studies have demonstrated that organic acids and amino acids exuded by plant roots can enhance the dissolution of metal oxide NPs (46). Compared with those in the ZnO group, the increased levels of carboxylic acids observed in the HWs+ZnO group (Fig. 2B) may reveal the mechanism by which the HWs enhanced ZnO NP dissolution on the leaf surface (Fig. 2E).

**Uptake and Translocation of ZnO NPs within Leaves under HW Conditions.** Dissolved Zn ions can penetrate the cuticle or enter the leaf through stomatal cavities (47). Foliar application of ZnO NPs significantly increased the total and ionic Zn contents in the leaves by 169.7% and 43.4%, respectively, under ambient temperature conditions and by 115.2% and 46.8%, respectively, under HW conditions (Fig. 2F). The total Zn content in the rice leaves did not differ significantly between the ZnO group and the HWs+ZnO group (Fig. 2F). However, the ionic Zn content in the HWs+ZnO group was 1.22 times greater than that in the ZnO group (Fig. 2F), likely due to the increased dissolution of ZnO on the leaf surface (Fig. 2E). In contrast, the particulate Zn content in the leaves of the HWs+ZnO group was 23.8% lower than that in the ZnO group (Fig. 2F), which may be attributed to stomatal closure under HW conditions (24).

Single-particle inductively coupled plasma–mass spectrometry (sp-ICP–MS) was employed to assess the uptake of ZnO NPs within leaves (Fig. 2 G and H and *SI Appendix*, Fig. S12). The sizes of the ZnO NPs detected in the leaves ranged from approximately 50 to 160 nm (Fig. 2 G and H), making these NPs larger than the pristine ZnO NPs (approximately 30 to 80 nm, *SI Appendix*, Fig. S13), suggesting the formation of a biocorona on the ZnO surface after leaf uptake. After entering the leaves, the ZnO NPs accumulated within mesophyll cells (Fig. 2I). Subsequently, the ZnO NPs may be transported to the phloem via two possible pathways: the apoplastic pathway, which involves movement between cells and/or within the cell wall, and the symplastic pathway, which involves transport through the cytoplasm (48). The phloem system is crucial in the translocation and dissolution

of foliar-sprayed ZnO NPs (49). The dissolution curve of the ZnO NPs in simulated phloem sap revealed that the content of dissolved ions gradually increased over 6 d (*SI Appendix*, Fig. S11). However, no significant difference in the dissolved Zn content was observed between the ZnO-treated group and the HWs+ZnO-treated group (*SI Appendix*, Fig. S11), suggesting that short-term (6 d) HW treatment had no effect on the ZnO NP dissolution in simulated phloem sap. The  $\zeta$ -potential of the ZnO NPs in simulated phloem sap ( $-9.7 \pm 0.3\text{ mV}$  at ambient temperature and  $-9.2 \pm 0.3\text{ mV}$  under HW conditions) was significantly greater than those in MQ water ( $-20.8 \pm 3.8\text{ mV}$  at ambient temperature and  $-18.5 \pm 1.2\text{ mV}$  under HW conditions) (*SI Appendix*, Fig. S14). This is likely due to electrostatic interactions between the negatively charged ZnO NPs and the positively charged ions ( $\text{K}^+$ ,  $\text{Mg}^{2+}$ , and  $\text{Na}^+$ ) in the simulated phloem sap. The hydrodynamic diameters of the ZnO NPs in simulated phloem sap were greater than those in MQ water, which may be correlated with the formation of a biocorona (e.g., amino acids and sugars) on the NP surface (*SI Appendix*, Fig. S14). Moreover, compared with that at ambient temperature, HW conditions significantly reduced the hydrodynamic diameter of the ZnO NPs in phloem sap (*SI Appendix*, Fig. S14). This reduction may be attributed to differences in biocorona formation at ambient temperature and under HW conditions.

The Zn content in the unsprayed leaves was not determined via EDS analysis (*SI Appendix*, Fig. S15). After foliar application of ZnO NPs under ambient temperature conditions, Zn was predominantly localized within the epidermal layer and palisade mesophyll cells (Fig. 2J). However, under HW conditions, Zn was detectable within both palisade and spongy mesophyll cells (Fig. 2J), indicating that HWs accelerated the translocation of ZnO NPs within leaves; however, this phenomenon needs further investigation. Previous research has demonstrated that ZnO NPs accumulated within mesophyll tissue and then released  $\text{Zn}^{2+}$  ions following foliar application of ZnO NPs (24). This study further reveals that foliar-applied ZnO NPs penetrate the leaves in both the ionic Zn and particulate forms. Additionally, compared with ambient temperature conditions, HWs increased the dissolved Zn content in the leaves and facilitated the transport of ZnO NPs from the surface to the mesophyll cells to meet the increased Zn demands of plants under HW conditions (50).

**The Increase in Nutrient Contents Contributed to the Improvement in and Protection of Photosynthesis under HW Conditions.** Under HW conditions, foliar application of ZnO NPs significantly increased the contents of manganese (Mn), copper (Cu), iron (Fe), and magnesium (Mg) in the leaves by 26.3%, 416.9%, 86.2%, and 15.8%, respectively (Fig. 3A–D). This increased accumulation of macro- and micronutrients may be attributed to increased demand from the stimulation of plant metabolic processes. Importantly, Mg and Zn contribute to chlorophyll synthesis (51). Foliar application of ZnO NPs increased the chlorophyll a/b content by 26.1%/19.9% at ambient temperature and 22.2%/24.8% under HW conditions, respectively (Fig. 3E). However, HW conditions resulted in a 17.9% reduction in chlorophyll b content (Fig. 3E). Ribulose-1,5-bisphosphate carboxylase/oxygenase (Rubisco), a pivotal enzyme involved in carbon fixation during photosynthesis that plays a key role in determining crop yield, is influenced by elevated concentrations of metals (Mn, Mg, Zn, Fe, and Cu) in crops and increases their oxygenation activity (52). Foliar application of ZnO increased Rubisco activity by 21.2% under HW conditions, whereas HW treatment alone decreased Rubisco activity by 12.1% (Fig. 3F). Mn, Cu, Fe, and Zn also constitute integral components of plant photosynthetic electron transport proteins (53). ZnO NPs increased

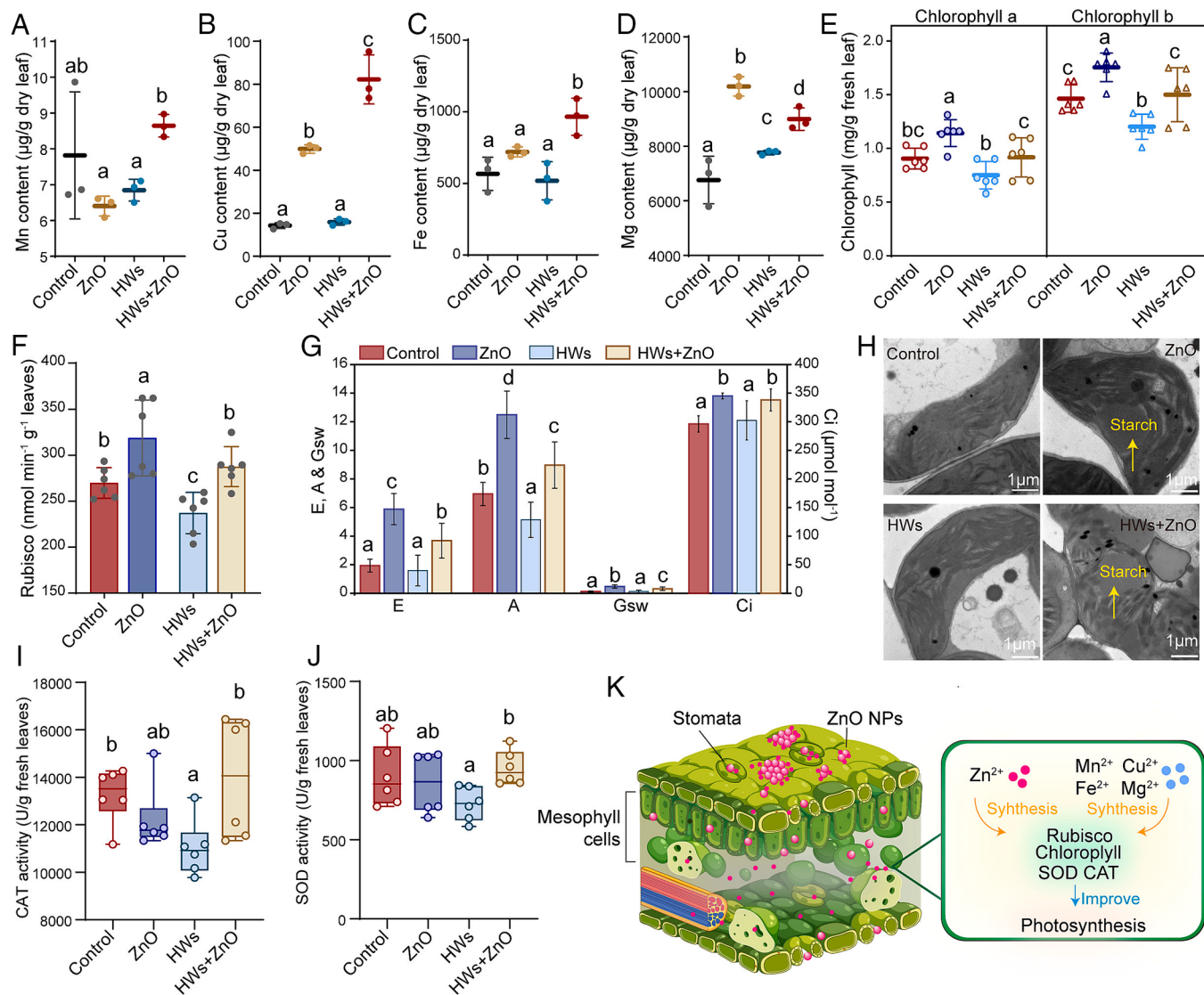


**Fig. 3.** Photosynthesis and antioxidant enzymes in rice leaves. Contents of (A) Mn, (B) Cu, (C) Fe, and (D) Mg in rice leaves. (E) Chlorophyll contents in rice leaves. (F) Rubisco activities in rice leaves. (G) Photosynthetic parameters, including the transpiration rate ( $E$ ,  $\text{mmol}/\text{m}^2\cdot\text{s}$ ), stomatal conductance ( $\text{G}_{\text{sw}}$ ,  $\text{mol}/\text{m}^2\cdot\text{s}$ ), intercellular carbon dioxide concentration ( $\text{Ci}$ ,  $\mu\text{mol}/\text{mol}$ ), and net photosynthetic rate ( $A$ ,  $\mu\text{mol}/\text{m}^2\cdot\text{s}$ ). (H) TEM images of chloroplasts. (I) CAT contents in rice leaves. (J) SOD contents in rice leaves. (K) Schematic showing the accumulation of ZnO NPs and improved photosynthesis in leaves. The data are presented as the means of three (A–D) or six (E–G, I, and J) replicates  $\pm$  the SD. Different lowercase letters denote a statistically significant difference based on LSD pairwise comparisons ( $P < 0.05$ ).

the transpiration rate, stomatal conductance, and intercellular carbon dioxide concentration by 204.2% and 132.0%, 276.6% and 145.4%, and 16.5% and 11.9%, respectively, at ambient temperature and under HW conditions (Fig. 3G). Notably, stomatal conductance in the HWs+ZnO group was significantly lower than that in the ZnO group (Fig. 3G). Since ZnO NPs penetrate the leaf epidermis through the stomata (24), the uptake of ZnO NPs by the leaves was reduced by HW treatment (Fig. 2F). The net photosynthetic rate increased by 79.3% and 74.4% at ambient temperature and under HW conditions, respectively, owing to ZnO NP application, whereas HWs led to a 26.2% decrease (Fig. 3G). The content of starch, which acts as a reservoir for photosynthetic carbohydrates, decreased by 16.5% under HW conditions, whereas foliar application of ZnO NPs led to increases in starch contents of 29.8% and 28.7% at ambient temperature and under HW conditions, respectively (SI Appendix, Fig. S16). The transmission electron microscopy (TEM) images revealed that starch granules accumulated within the chloroplasts of the

ZnO- and HWs+ZnO-treated leaves, which is indicative of robust photosynthetic activity (Fig. 3H).

HVs caused the catalase (CAT) content to decrease by 17.0% with a concurrent increase in the  $\text{H}_2\text{O}_2$  content of 78.5% (Fig. 3I and SI Appendix, Fig. S17A). However, under HW conditions, ZnO application increased the CAT and superoxide dismutase (SOD) contents by 26.7% and 31.2%, respectively, while decreasing the hydrogen peroxide ( $\text{H}_2\text{O}_2$ ) and superoxide anion radical ( $\text{O}_2^-$ ) contents by 26.3% and 42.4%, respectively (Fig. 3I and J and SI Appendix, Fig. S17 A and B). Excessive reactive oxygen species (ROS) impair the photosynthetic system, whereas antioxidant enzymes protect the photosynthetic process from the detrimental effects of free radicals (54, 55). Both Zn and Cu serve as active centers of antioxidative enzymes (56). Taken together, these data indicate that the foliar application of ZnO NPs increased the levels of micro- and macronutrients in the leaves, which became integrated with chlorophyll and key enzymes involved in photosynthesis and the antioxidant system, contributing to improved photosynthesis (Fig. 3K).

**Under HW Conditions, ZnO NPs Reversed Photosynthesis and Antioxidant System Transcriptomic Dysregulation.** PCA revealed separations between HWs and controls, as well as between HWs+ZnO and HWs (Fig. 4A and B). Analyses of the differentially expressed genes (DEGs) revealed 1,027, 601, and 993 DEGs in the HW/control, ZnO/control, and HWs+ZnO/HWs comparisons, respectively (Fig. 4C). Gene Ontology enrichment analysis revealed that antioxidant activity, secondary metabolite biosynthetic processes, carbohydrate metabolic processes, and heme binding pathways were enriched in the DEGs identified in the above comparison groups (Fig. 4D). Notably, compared with that in the HW group, the expression levels of relevant genes in the HWs+ZnO group were more similar to those in the normal (control) group (Fig. 4D). In addition, nearly half of the DEGs were identified in the HWs+ZnO/HWs vs. HWs/control comparisons (Fig. 4E), indicating that ZnO NPs reversed the transcriptional dysregulation induced by HW conditions. The expression levels of genes related to the tetrapyrrole binding pathway were widely downregulated by HWs but widely upregulated by ZnO NPs under HW conditions (Fig. 4F). Moreover, ZnO NPs upregulated the Mg transporter-related genes *Os02g0518000* and *Os03g0396100* (Fig. 4G), which in turn induced an increase in the Mg contents in the leaves (Fig. 3D). Chlorophylls are Mg<sup>2+</sup>-containing tetrapyrrole compounds (51); thus, the

upregulation of genes associated with tetrapyrrole binding and the Mg transporter improved the synthesis of chlorophyll (Fig. 3E). Similarly, the relative expression of photosynthesis genes (*rbcS*, *psbR*, and *psbS*) was significantly greater in the HWs+ZnO group than in the HW group, whereas the expression of both *rbcS* and *psbR* was significantly lower in the HW group than in the control group (Fig. 4H). *RbcS* encodes the enzyme Rubisco for carbon fixation (57); *psbR* functions in anchoring oxygen-evolving complex proteins to photosystem II; and *psbS* is critical in regulating nonphotochemical chlorophyll fluorescence quenching (58, 59). Taken together, the results here suggested that the ZnO NPs corrected the transcriptomic dysregulation of chlorophyll synthesis and photosynthesis induced by HWs, thereby improving photosynthesis.

There was enrichment in DEGs in the nutrient reservoir activity pathway, which presented greater expression in the HWs+ZnO group than in the HW group (Fig. 4I), consistent with the increase in nutrient contents observed in the leaves (Fig. 3 A–D). The expression of genes involved in antioxidant activity was widely upregulated by ZnO NPs under HW conditions but not significantly altered by HW treatments alone (Fig. 4J), which is consistent with the observed trends in antioxidant enzyme activities (Fig. 3J). In addition, foliar application of ZnO NPs regulated the expression of Zn and Fe transporters (SI Appendix, Fig. S18). Our

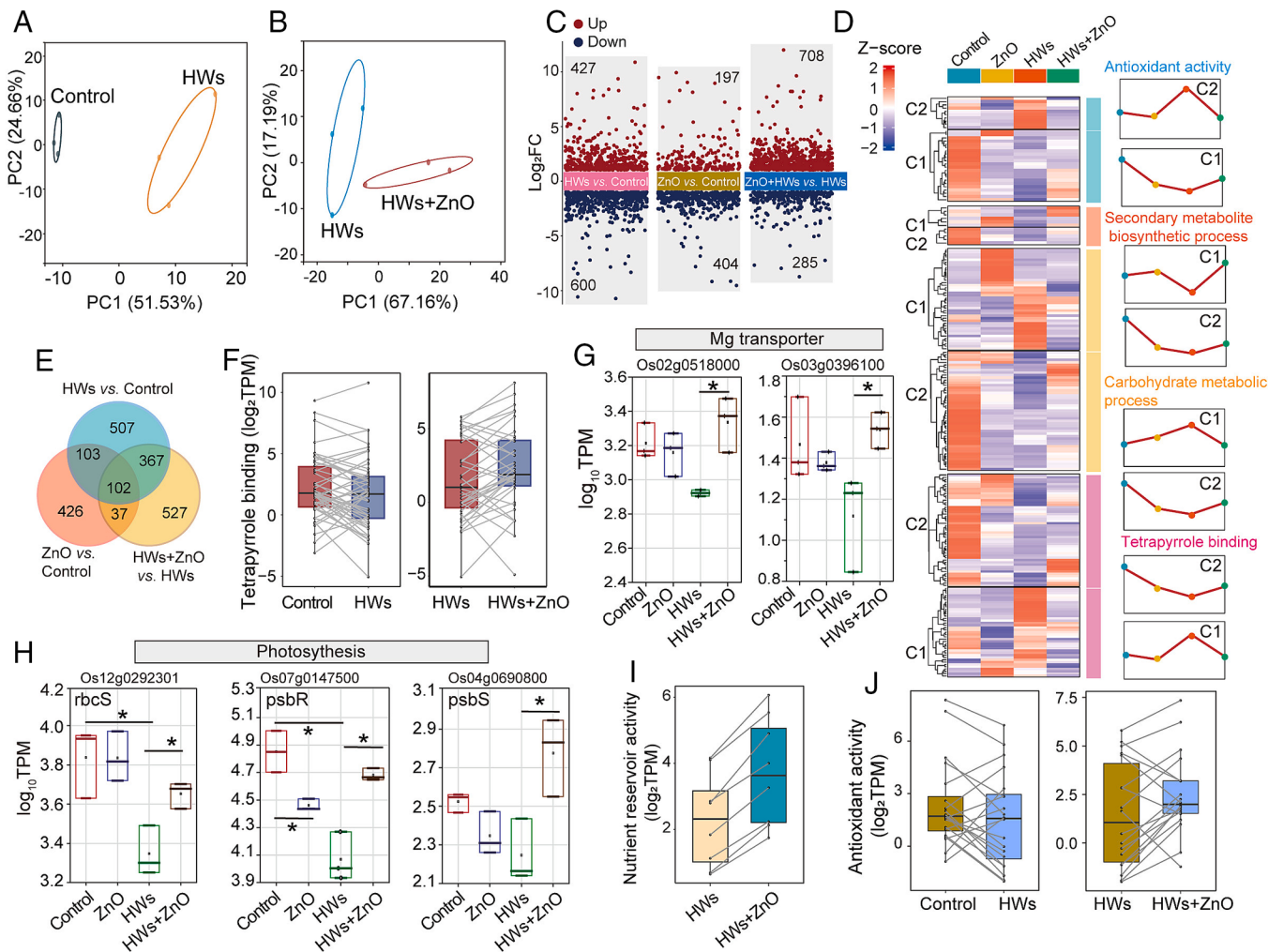


**Fig. 4.** Transcriptional responses of rice leaves to ZnO NPs and HWs. PCA plots of rice leaves comparing the following groups: (A) HWs and control and (B) HWs+ZnO and HWs. (C) DEG analysis showing up- and downregulated genes in the HWs/control, ZnO/control, and HWs+ZnO/HWs comparisons. (D) Heatmaps of the DEGs. (E) Venn diagram showing the DEGs in the HWs/control, ZnO/control, and HWs+ZnO/HW comparisons. (F) Expression patterns of DEGs in pathways related to tetrapyrrole binding. (G) Expression of genes related to the Mg transporter. (H) Expression of genes related to photosynthesis. (I) Expression patterns of DEGs in pathways related to nutrient reservoir activity. (J) Expression patterns of DEGs in pathways related to antioxidant activity. The data are presented as the means of three (G and H) replicates  $\pm$  the SD. Means labeled with asterisks indicate DEGs between treatments.

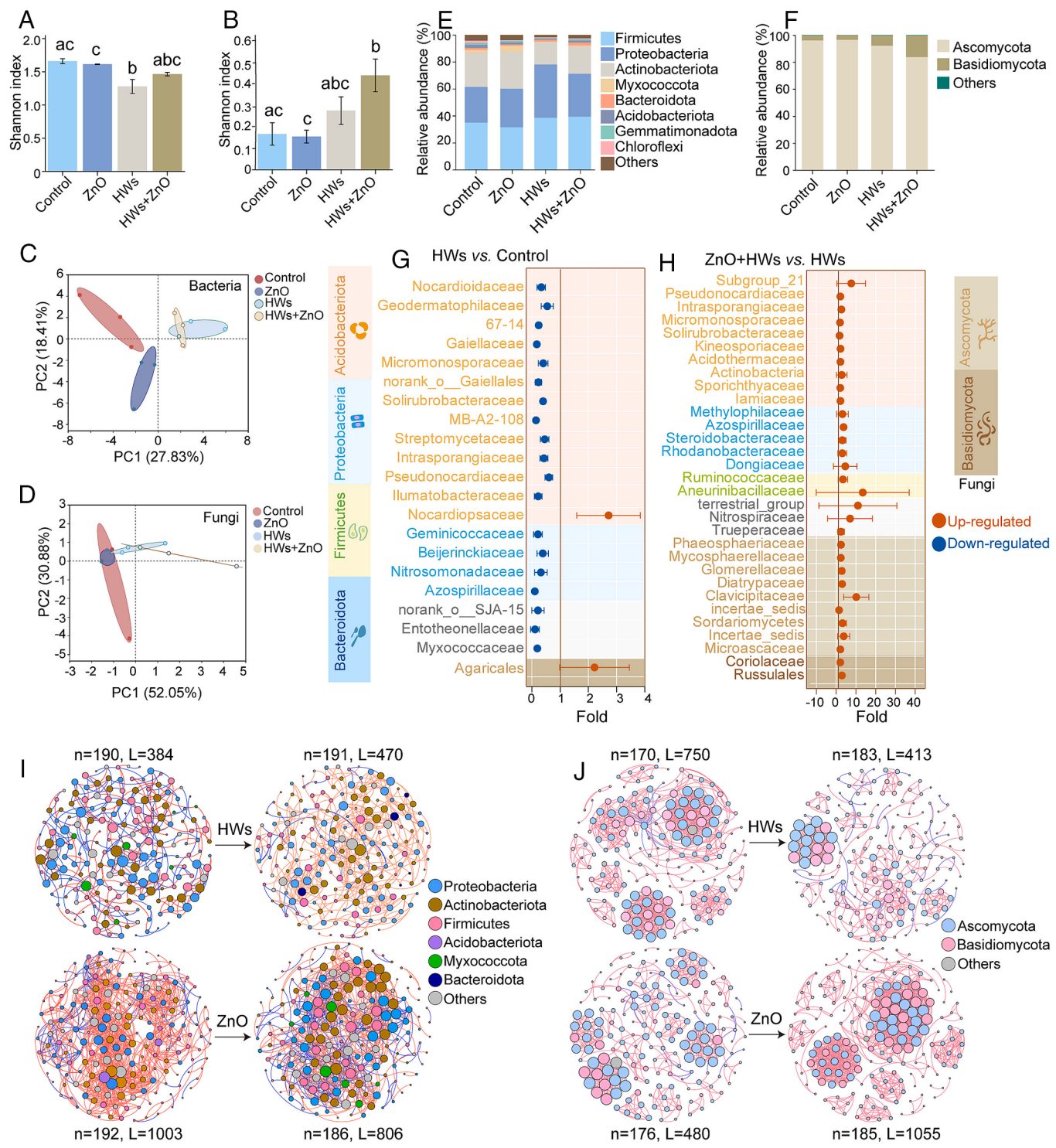


**Fig. 5.** Responses of the phyllosphere microbial community to ZnO NPs and HWs. Shannon indices of (A) bacteria and (B) fungi at the phylum level. PCA plots of (C) bacteria and (D) fungi. Relative abundance of the (E) top eight bacterial phyla and (F) top two fungal phyla. The top 20 families of bacteria and fungi that were significantly altered in the (G) HWs/control and (H) HWs+ZnO/HWs comparisons. (I) Co-occurrence networks of the top 200 bacterial genera under ambient temperature conditions, under HW conditions, in the ZnO-free group and in the ZnO-treated group. (J) Co-occurrence networks of the top 200 fungal genera under ambient temperature conditions, under HW conditions, in the ZnO-free group and in the ZnO treatment group. Fungal and bacterial genera are shown as nodes, and the node size is positively correlated with the number of edges connected to each node. Red edges indicate positive correlations, whereas the blue lines indicate negative correlations. The data are presented as the means of three (A and B) replicates  $\pm$  the SD. Different lowercase letters indicate that the difference is significant on the basis of Kruskal-Wallis comparisons combined with Tukey-Kramer (0.95) comparisons.

results confirmed that the regulation of metal transporters by ZnO led to the accumulation of micro- and macronutrients (Zn, Fe, and Mg) in leaves (Figs. 2F and 3 C and D), and these accumulated nutrients participated in the protection of and improvement in photosynthesis.

**ZnO NPs Protected the Phyllosphere Microbial Community from HW Damage.** HWs significantly decreased the Shannon index of bacteria at the phylum level (Fig. 5A). Under HW conditions, ZnO NPs increased the Shannon indices of both bacteria and fungi (Fig. 5 A and B), indicating increased microbial diversity.

Leaf microbial diversity is positively correlated with plant productivity (60). Under HW conditions, ZnO NPs did not significantly affect the microbial structure (Fig. 5 C and D). Compared with that in the control treatment, the abundance of Chloroflexi in the HW group significantly decreased by 80.6% (Fig. 5E). Conversely, compared with that in the HW group, the abundance of Chloroflexi in the HWs+ZnO group increased by 102.7% (Fig. 5E). Chloroflexi phototrophs lead to an increase in the chlorophyll content in plants (61), which partly contributed to the increased chlorophyll level in rice leaves (Fig. 3E). Neither HWs nor ZnO NPs alone significantly altered the fungal composition at the phylum level (Fig. 5F). A Student's *t* test was also conducted to determine whether there were significant changes in the bacterial and fungal taxa (Fig. 5 G and H). Notably, the number of distinguished taxa decreased widely in response to HWs alone (Fig. 5G); however, the number of taxa with a significant change in abundance strongly increased with ZnO NP application under HW conditions (Fig. 5H), indicating that the ZnO NPs protect the phyllosphere microbial community under HW stress. The abundance of Pseudonocardiaceae, which is positively correlated with the plant Fe concentration in *Solanum nigrum* L. (62), was greater in the HWs+ZnO group than in the HW group but lower in the HW group than in the control, which is consistent with the Fe concentration in the rice leaves (Fig. 3C). In addition, the abundances of Solirubrobacteraceae, Actinobacteria, Azospirillaceae, Rhodanobacteraceae, and Aneurinibacillaceae, which are widely considered promoters of crop production, were increased by ZnO NPs under HW conditions but partly decreased by HW conditions alone compared with those in the control (Fig. 5 G and H). HWs increased the relative frequency of positive correlations between bacterial taxa, whereas ZnO NPs increased the relative frequency of negative correlations (Fig. 5I). Negative associations between microorganisms promote community stability (63). In addition, ZnO treatment increased the number of highly connected taxa (Fig. 5J), indicating increased microbial stability (64). A co-occurrence network analysis of fungal genera revealed that HWs decreased the number of edges by 44.9%, whereas ZnO increased the number of edges by 119.8% (Fig. 5J), suggesting that microbial complexity decreased upon HW treatment but increased with ZnO NP application.

A previous study demonstrated that foliar application of ZnO NPs (0.25 mg per plant) to 10-d-old pumpkin seedlings resulted in a 24.4% increase in plant biomass, enhanced soil microbial community diversity, and improved microbiome composition (31). In the phyllosphere, foliar application of ZnO NPs (4 mg per plant) to 80-d-old rice leaves protected phyllosphere microorganisms from HW damage, increased microbial diversity, stability, and complexity, and promoted beneficial microbiomes (Fig. 5). The altered microbial community contributed to the increases in metal content, chlorophyll synthesis, and grain yield. A significant correlation was found between leaf surface metabolites and the phyllosphere microbial phylum in this study (SI Appendix, Fig. S19). Leaf surface exudates influence the composition, structure, and diversity of phyllosphere microorganisms (65). For example, volatile organic compounds, such as benzenoids, promote the growth of beneficial microbes while inhibiting the establishment of harmful microbes, thereby allowing plants to regulate microbial colonization on their surfaces (66). Moreover, carboxylic acids shape the composition and structure of the phyllosphere microbial community by replenishing nutrients for the phyllosphere microbiota (67). Therefore, ZnO NPs may regulate the phyllosphere microbial community by altering leaf exudates and forming an eco-corona. Foliar application of Zn<sup>2+</sup> ions increased the diversity of the bacterial community but not the diversity of the fungal community or the complexity and stability of the microbial

community (SI Appendix, Fig. S20). These findings suggest that the protective effects provided by the ZnO NPs on phyllosphere microorganisms under HW conditions cannot be attributed entirely to ZnO NP dissolution. A potential mechanism for these effects is that the aggregated ZnO NPs on the leaf surface (Fig. 2A) may provide sites for microbiome colonization, similar to microplastics and dust particles (68).

## Conclusions

The stresses from the increasing population and climate change threaten global food security. In this study, foliar-applied ZnO NPs were found to penetrate the leaves as both ionic Zn and in its particulate form. ZnO NPs aggregated on the leaf surface and interacted with leaf surface molecules. Compared with ambient temperature conditions, HWs significantly increased the dissolution of ZnO NPs on the leaf surface and facilitated their transport from the surface to mesophyll cells. Compared with the HW control, HWs+ZnO effectively increased grain yield and nutritional quality by increasing plant photosynthesis, improving nutrient uptake, and shaping the phyllosphere microbial community (SI Appendix, Fig. S21). Notably, this study reveals that ZnO NPs have protective effects on the phyllosphere microbial community under HW conditions, suggesting a promising way to maintain the diversity and stability of the phyllosphere microbial community under extreme climate events through nanotechnology. In summary, this study reveals extreme events as factors influencing the dissolution and translocation of ZnO NPs and the subsequent biological response and highlights that applying ZnO NPs to the leaves of crops holds promise for alleviating the global food crisis in the face of an increasing population and climate change.

## Methods

**Plant Growth and Treatment.** Rice plants (*Oryza sativa* L. spp. *japonica*) were cultivated in a greenhouse. Details regarding the rice cultivation process are provided in SI Appendix, Text S1. The ZnO NPs were purchased from Nanjing XFNANO Materials Tech Co., Ltd. (Nanjing, China) with diameters ranging from 30 to 80 nm, which was verified via TEM (SI Appendix, Fig. S13). Composition analysis via X-ray photoelectron spectroscopy confirmed the presence of Zn and O (SI Appendix, Fig. S22). The simulation of HW conditions (37 °C) was based on local temperature records (SI Appendix, Fig. S23) and established methodologies from previous research (69), as detailed in SI Appendix, Text S2.

**Rice Seedling Test.** Rice plants were planted in plastic pots (two plants/pot) with three replicates per treatment and cultivated for 21 d. Given the agricultural application of ZnO NPs, it may be more practical to apply ZnO NPs during HW events rather than attempting to apply ZnO NPs in advance. Additionally, temperature is known to affect the uptake of NPs by leaves and their dissolution, and the NP content in plants is a crucial factor that influences their biological effects (70, 71). To investigate how HW events regulate the dissolution and translocation of ZnO NPs, as well as their subsequent biological effects, MQ water, ZnO NPs (50 mg/L, 100 mg/L, or 200 mg/L), or an equivalent concentration of Zn<sup>2+</sup> ions (100 mg/L, 200 mg/L, or 400 mg/L ZnSO<sub>4</sub>) were sprayed on rice leaves daily (0.5 mL per plant/d) before HW treatment during the 6-d HW period; ambient temperature served as the control. After 6 d of treatment, the rice seedlings were collected, thoroughly washed with distilled water, 2% HNO<sub>3</sub>, and 3% ethanol to eliminate surface-attached NPs, and subsequently dried in an oven at 80 °C. The shoots were separated and weighed, while the stems and leaves were ground for subsequent analysis of the Zn and starch contents.

For Zn content analysis (three replicates), 20 mg of dried leaves was digested with a mixture comprising 1 mL of 30% H<sub>2</sub>O<sub>2</sub> and 3 mL of 68% HNO<sub>3</sub> at 180 °C for 30 min, followed by dilution to 10 mL with distilled water. The digested samples were then analyzed via ICP-MS (Perkin Elmer, Elan Cruz-e, USA). The quality control (QC) and quality assurance (QA) requirements of the digestion method and the ICP-MS analysis are presented in SI Appendix, Text S3.

A starch assay kit (G0507 W, Suzhou Grace Biotechnology Co., Ltd., China) was used for starch content analysis (six replicates) according to the manufacturer's instructions.

**Full Life Cycle Experiment.** To assess the potential of ZnO NPs to increase agricultural production during HW days or at ambient temperature, we conducted a full life cycle experiment. Given the input of ZnO fertilizer and its ability to promote rice growth, a concentration of 100 mg/L ZnO NPs was selected for the experiment. Consistent with the seedling experiment, HW treatment was applied daily following the foliar spray of ZnO NPs (100 mg/L, 6.7 mL per plant/d). Details regarding the treatment and harvest of the rice plants are provided in *SI Appendix, Text S4*.

**Fluorescence Labeling and Confocal Laser Scanning Microscopy (CLSM) Imaging.** The NPs were labeled with fluorescein isothiocyanate (FITC) according to previous methods (24). The FITC-labeled ZnO NPs were subsequently applied to rice leaves via a spraying technique. The leaves were then collected and visualized via CLSM (LSM880, Carl Zeiss, Germany) with an excitation wavelength of 488 nm and an emission wavelength of 525 nm, as detailed in *SI Appendix, Text S5*.

**Photosynthetic Parameters.** The photosynthetic rate, transpiration rate, intercellular CO<sub>2</sub> concentration, and stomatal conductance (six replicates) were measured via a portable photosynthesis measurement system (Li-COR LI-6800, LI-COR, USA) in accordance with the manufacturer's instructions. Throughout the measurements, the ambient CO<sub>2</sub> concentration was held constant at 400 μmol/mol, while the air temperature was maintained at 26 °C.

**ICP-MS.** Rice leaves were segregated to determine the contents of Cu, Mg, Fe, and Mn; the experimental methodology has been previously described for the above seedling experiments. The QC and QA requirements of the digestion method and the ICP-MS analysis are presented in *SI Appendix, Text S3*.

**Fourier transform infrared (FTIR) Spectroscopy of the ZnO NPs and Rice Leaves.** The functional groups of the rice leaves and the ZnO NPs on the leaf surface were analyzed via FTIR spectroscopy (Nicolet iS50, THERMO, USA), as detailed in *SI Appendix, Text S6*.

**Leaf Surface Roughness and Wettability Measurements.** Leaf surface roughness and wettability were measured via CLSM (VK-X1000, Keyence, Japan) and a contact angle goniometer (JY-82C, Dingsheng, China), respectively, as detailed in *SI Appendix, Text S7*.

**ZnO Deposition and Dissolution on the Leaf Surface.** The total Zn and dissolved Zn contents on the leaf surface were determined via ICP-MS (Perkin Elmer, Elan Cruz-e, USA), as detailed in *SI Appendix, Text S8*.

**ZnO Dissolution within the Leaves.** A methanol-based digestion protocol was used to assess NP uptake by rice leaves (72). The detailed digestion protocol and sp-ICP-MS (NexION 1000G, PerkinElmer, USA) parameters are provided in *SI Appendix, Text S9*. The total Zn, dissolved Zn, and particulate Zn contents in the rice leaves were quantified via ICP-MS (Perkin Elmer, Elan Cruz-e, USA), as detailed in *SI Appendix, Text S9*.

**Release of Dissolved Zn from ZnO NPs in Distilled Water and Simulated Phloem Sap.** ZnO suspensions (10 mg/L, three replicates) were prepared in distilled water or simulated phloem sap in 50 mL tubes. The ζ-potentials and hydrodynamic diameters of the ZnO NPs (10 mg/L) were measured via dynamic light scattering (Malvern Instruments, UK). The contents of dissolved Zn were analyzed via ICP-MS (Perkin Elmer, Elan Cruz-e, USA), as detailed in *SI Appendix, Text S10*.

**Analysis of Metabolites on the Leaf Surface.** After 6-d of HW and ZnO treatment, rice leaves (three replicates) were collected. Leaf surface metabolites were extracted and analyzed following established protocols (73). The metabolites were analyzed via an ultrahigh-performance liquid chromatography system (Ultimate 3000, Thermo Fisher Scientific, USA) coupled to a high-resolution mass spectrometer (Orbitrap Fusion, Thermo Fisher Scientific, USA). Details regarding the extraction and analysis of the leaf surface metabolites are provided in *SI Appendix, Text S11*.

**TEM and Scanning electron microscopy (SEM) Observations.** Rice leaves were examined via TEM (JEM1200EX, JEOL, Japan) and SEM (JSM-7800F, JEOL, Japan) with an EDS system, as detailed in *SI Appendix, Text S12*.

**Starch, Chlorophyll, Rubisco Activity, ROS, and Antioxidant Enzyme Analyses.** The starch analysis (six replicates) procedure was performed according to the methods described in the above seedling experiment. Chlorophyll pigments were analyzed with an ultraviolet (UV) spectrophotometer (UV-2600, SHIMADZU, Japan), as detailed in *SI Appendix, Text S13*. The Rubisco activity (six replicates) was measured with an ELISA kit (G0602F24, Grace, China) according to the manufacturer's instructions. The analysis of antioxidant enzymes (six replicates), including CAT and SOD, from the leaf samples was performed via the G0105 W and G0107 W assay kits (Suzhou Grace Biotechnology Co., Ltd., China), respectively, following the manufacturer's protocols. The levels of H<sub>2</sub>O<sub>2</sub> and O<sub>2</sub><sup>•-</sup> (six replicates) were analyzed via an H<sub>2</sub>O<sub>2</sub> assay kit (AK305, Bioss, China) and an O<sub>2</sub><sup>•-</sup> assay kit (T01121, Leigen, China), respectively, following the manufacturer's protocols.

**Transcriptomic Analysis.** Three replicates of each treatment were used for the transcriptome study. Rice leaves were collected and preserved at -80 °C. Transcriptomic analysis was carried out at Shanghai Majorbio Bio-Pharm Technology Co., Ltd., China. The extraction of leaf RNA, preparation of the transcriptome library, synthesis of complementary deoxyribonucleic acid, and sequencing are described in *SI Appendix, Text S14*.

**Phyllosphere Microbial Analysis.** After 6 d of exposure to HWs plus ZnO NPs, the leaves (three replicates) were collected and placed in 50 mL sterile tubes. The collection and sequencing of the phyllosphere microorganisms are detailed in *SI Appendix, Text S15*. The ZnO solution (100 mg/L) was filtered through a 10 kDa Amicon Ultra15 Centrifugal Filter unit. The filtrates and ZnO NPs (100 mg/L) were then individually sprayed onto the rice leaves as described above. After 6 d of combined exposure (HWs and ZnO NPs/Zn<sup>2+</sup>), the leaves (three replicates) were collected for analysis of the phyllosphere microorganisms as described above.

**Panicle.** After harvesting, the grain weight per plant was documented from six replicates. Then, the extractable protein fractions were quantified via a Bradford protein assay kit (P0006, Beyotime Biotechnology, China). Details regarding the extraction of soluble protein are provided in *SI Appendix, Text S16*. The free amino acids were assessed via an automatic amino acid analyzer (S-433D, Sykam, Germany), and the details are provided in *SI Appendix, Text S17*.

**Statistical Analysis.** The data are expressed as the means ± SD of at least three replicate experiments. The significance of differences between treatments was analyzed via one-way ANOVA followed by least significant difference (LSD) pairwise comparisons in SPSS 25 (SPSS, Inc., Chicago, IL, USA). A *P* value < 0.05 was considered to indicate statistical significance and is indicated by different letters or asterisks.

**Data, Materials, and Software Availability.** Raw sequencing data are available at [https://pan.baidu.com/s/1pMcRe\\_pxygfM0MgKqNqQiAw?pwd=3q3q](https://pan.baidu.com/s/1pMcRe_pxygfM0MgKqNqQiAw?pwd=3q3q) (74). All study data are included in the article and/or *SI Appendix*.

**ACKNOWLEDGMENTS.** This work was financially supported by the National Natural Science Foundation of China (grant no. U22A20615), the 111 program (grant no. B17025), and Fundamental Research Funds for the Central Universities. We thank Freepik for designing the vector elements.

Author affiliations: <sup>a</sup>Key Laboratory of Pollution Processes and Environmental Criteria (Ministry of Education)/Carbon Neutrality Interdisciplinary Science Centre, College of Environmental Science and Engineering, Nankai University, Tianjin 300350, China; and <sup>b</sup>Stockbridge School of Agriculture, University of Massachusetts, Amherst, MA 01003

1. M. van Dijk, T. Morley, M. L. Rau, Y. Saghai, A meta-analysis of projected global food demand and population at risk of hunger for the period 2010–2050. *Nat. Food* **2**, 494–501 (2021).
2. J. Du, W. Liu, Q. Zhou, Combating the food crisis and farmland contamination with safe farming practices. *J. Agric. Food Chem.* **72**, 15053–15054 (2024).
3. B. Gu *et al.*, Cost-effective mitigation of nitrogen pollution from global croplands. *Nature* **613**, 77–84 (2023).
4. H. Guo, J. C. White, Z. Wang, B. Xing, Nano-enabled fertilizers to control the release and use efficiency of nutrients. *Curr. Opin. Environ. Sci. Health* **6**, 77–83 (2018).

5. X. Xu *et al.*, Global greenhouse gas emissions from animal-based foods are twice those of plant-based foods. *Nat. Food* **2**, 724–732 (2021).
6. A. K. Jain, Greenhouse gas emissions from nitrogen fertilizers. *Nat. Food* **4**, 139–140 (2023).
7. T. Wheeler, J. von Braun, Climate change impacts on global food security. *Science* **341**, 508–513 (2013).
8. D. Renard, L. Mahaut, F. Noack, Crop diversity buffers the impact of droughts and high temperatures on food production. *Environ. Res. Lett.* **18**, 045002 (2023).
9. D. Gao *et al.*, Association between extreme ambient heat exposure and diabetes-related hospital admissions and emergency department visits: A systematic review. *Hyg. Environ. Health Adv.* **4**, 100031 (2022).
10. WMO, Guidelines on the definition and monitoring of extreme weather and climate events. WMO. [https://rcc.dwd.de/DWD-RCC/EN/overview/documents/01\\_wmo\\_guidelines.pdf?sessionid=F5BA3D1D14E12B33CB41304CF1B6FB1.live2](https://rcc.dwd.de/DWD-RCC/EN/overview/documents/01_wmo_guidelines.pdf?sessionid=F5BA3D1D14E12B33CB41304CF1B6FB1.live2). Accessed 10 March 2024.
11. M. Gao *et al.*, Large-scale climate patterns offer preseasonal hints on the co-occurrence of heat wave and O<sub>3</sub> pollution in China. *Proc. Natl. Acad. Sci. U.S.A.* **120**, e2218274120 (2023).
12. D. Wang *et al.*, Nano-enabled pesticides for sustainable agriculture and global food security. *Nat. Nanotechnol.* **17**, 347–360 (2022).
13. C. Wang *et al.*, Carbon dots improve nitrogen bioavailability to promote the growth and nutritional quality of soybeans under drought stress. *ACS Nano* **16**, 12415–12424 (2022).
14. P. Deng *et al.*, Development potential of nanoenabled agriculture projected using machine learning. *Proc. Natl. Acad. Sci. U.S.A.* **120**, e2301885120 (2023).
15. Y. Yu *et al.*, Closing the gap between climate regulation and food security with nano iron oxides. *Nat. Sustain.* **7**, 758–765 (2024).
16. T. N. V. K. V. Prasad *et al.*, Nanoparticulate silica internalization and its effect on the growth and yield of groundnut (*Arachis hypogaea* L.). *Environ. Sci. Technol.* **57**, 5881–5890 (2023).
17. M. Sun *et al.*, ZnO quantum dots outperform nanoscale and bulk particles for enhancing tomato (*Solanum lycopersicum*) growth and nutritional values. *Sci. Total Environ.* **857**, 159330 (2023).
18. T. L. Read *et al.*, Zinc accumulates in the nodes of wheat following the foliar application of <sup>65</sup>Zn oxide nano- and microparticles. *Environ. Sci. Technol.* **55**, 13523–13531 (2021).
19. H. Singh *et al.*, Recent advances in the applications of nano-agrochemicals for sustainable agricultural development. *Environ. Sci. Proc. Imp.* **23**, 213–239 (2021).
20. M. Faizan *et al.*, Zinc oxide nanoparticles (ZnO-NPs) induce salt tolerance by improving the antioxidant system and photosynthetic machinery in tomato. *Plant Physiol. Bioch.* **161**, 122–130 (2021).
21. S. A. Sinclair *et al.*, Systemic upregulation of MTP2- and HMA2-mediated Zn partitioning to the shoot supplements local Zn deficiency responses. *Plant Cell* **30**, 2463–2479 (2018).
22. Z. Shahzad, H. Rouached, A. Rakha, Combating mineral malnutrition through iron and zinc biofortification of cereals. *Compr. Rev. Food Sci. Saf.* **13**, 329–346 (2014).
23. T. L. Read *et al.*, Investigating the foliar uptake of zinc from conventional and nano-formulations: A methodological study. *Environ. Chem.* **16**, 459–469 (2019).
24. J. Zhu *et al.*, Mechanism of zinc oxide nanoparticle entry into wheat seedling leaves. *Environ. Sci. Nano* **7**, 3901–3913 (2020).
25. X. Xu *et al.*, Physiological responses of pumpkin to zinc oxide quantum dots and nanoparticles. *Environ. Pollut.* **296**, 118723 (2022).
26. M. Sun *et al.*, Nanoscale ZnO improves the amino acids and lipids in tomato fruits and the subsequent assimilation in a simulated human gastrointestinal tract model. *ACS Nano* **17**, 19938–19951 (2023).
27. H. A. Kareem *et al.*, Nanosized zinc oxide (n-ZnO) particles pretreatment to alfalfa seedlings alleviate heat-induced morpho-physiological and ultrastructural damages. *Environ. Pollut.* **303**, 119069 (2022).
28. R. Sohrabi, B. C. Paasch, J. A. Liber, S. Y. He, Phyllosphere microbiome. *Annu. Rev. Plant Biol.* **74**, 539–568 (2023).
29. S. De Mandal, J. Jeon, Phyllosphere microbiome in plant health and disease. *Plants* **12**, 3481 (2023).
30. Y.-G. Zhu *et al.*, Impacts of global change on the phyllosphere microbiome. *New Phytol.* **234**, 1977–1986 (2022).
31. X. Xu *et al.*, Foliar applied ZnO quantum dots boost pumpkin (*Cucurbita moschata* Duch.) growth and positively alter endophytic and rhizosphere microbial communities. *ACS Sustain. Chem. Eng.* **11**, 8503–8516 (2023).
32. Z. Lv *et al.*, Nutrient strengthening of winter wheat by foliar ZnO and Fe<sub>3</sub>O<sub>4</sub> NPs: Food safety, quality, elemental distribution and effects on soil bacteria. *Sci. Total Environ.* **893**, 164866 (2023).
33. A. Farooq, N. Farooq, H. Akbar, Z. U. Hassan, S. H. J. A. Gheewala, A critical review of climate change impact at a global scale on cereal crop production. *Agronomy* **13**, 162 (2023).
34. P. Thuesombat, S. Hannongbua, S. Akasit, S. Chadchawan, Effect of silver nanoparticles on rice (*Oryza sativa* L. cv. KDM105) seed germination and seedling growth. *Ecotox. Environ. Safe* **104**, 302–309 (2014).
35. M. F. Seleiman *et al.*, Zinc oxide nanoparticles: A unique saline stress mitigator with the potential to increase future crop production. *S. Afr. J. Bot.* **159**, 208–218 (2023).
36. A. Avellan *et al.*, Critical review: Role of inorganic nanoparticle properties on their foliar uptake and in planta translocation. *Environ. Sci. Technol.* **55**, 13417–13431 (2021).
37. H. Sun *et al.*, Uptake, transformation, and environmental impact of zinc oxide nanoparticles in a soil-wheat system. *Sci. Total Environ.* **857**, 159307 (2023).
38. R. Ahmed *et al.*, Differential response of nano zinc sulphate with other conventional sources of Zn in mitigating salinity stress in rice grown on saline-sodic soil. *Chemosphere* **327**, 138479 (2023).
39. S. Heinicke, K. Frieler, J. Jägermeyer, M. Mengel, Global gridded crop models underestimate yield responses to droughts and heatwaves. *Environ. Res. Lett.* **17**, 044026 (2022).
40. Y. Ye, A. M. Reyes, C. Li, J. C. White, J. L. Gardea-Torresdey, Mechanistic insight into the internalization, distribution, and autophagy process of manganese nanoparticles in *capsicum annuum* L: Evidence from orthogonal microscopic analysis. *Environ. Sci. Technol.* **57**, 9773–9781 (2023).
41. Y. Yu, W. Dai, Y. Luan, Bio- and eco-corona related to plants: Understanding the formation and biological effects of plant protein coatings on nanoparticles. *Environ. Pollut.* **317**, 120784 (2023).
42. B. Ribeiro da Luz, Attenuated total reflectance spectroscopy of plant leaves: A tool for ecological and botanical studies. *New Phytol.* **172**, 305–318 (2006).
43. I. Kurniawaty, Y. Yulizar, H. S. Oktaviano, A. K. Rianto, One-pot synthesis and characterization of magnesium oxide nanoparticles prepared by calliandra calothyrsus leaf extract. *Int. J. Chem. Mater. Eng.* **18**, 7–13 (2024).
44. P. P. Pal, J. Manam, Photoluminescence and thermoluminescence studies of Tb<sup>3+</sup> doped ZnO nanorods. *Mater. Sci. Eng. B* **178**, 400–408 (2013).
45. N. Arahman, R. A. Fitri, A. Wirakusuma, A. Fahrina, M. R. Bilad, Adsorption performance of low-cost Java Plum leaves and guava fruits as natural adsorbents for removal of free fatty acids from coconut oil. *Int. J. Eng.* **32**, 1372–1378 (2019).
46. E. Spielman-Sun *et al.*, Nanoparticle surface charge influences translocation and leaf distribution in vascular plants with contrasting anatomy. *Environ. Sci. Nano* **6**, 2508–2519 (2019).
47. M. H. F. Gomes *et al.*, In vivo evaluation of Zn foliar uptake and transport in soybean using X-Ray absorption and fluorescence spectroscopy. *J. Agr. Food Chem.* **67**, 12172–12181 (2019).
48. X. Gao *et al.*, Application of ZnO nanoparticles encapsulated in mesoporous silica on the abaxial side of a *Solanum lycopersicum* leaf enhances Zn uptake and translocation via the phloem. *Environ. Sci. Technol.* **57**, 21704–21714 (2023).
49. S. Rodrigues *et al.*, Effect of a zinc phosphate shell on the uptake and translocation of foliarly applied ZnO nanoparticles in pepper plants (*Capsicum annuum*). *Environ. Sci. Technol.* **58**, 3213–3223 (2024).
50. W. Han, L. Huang, O. J. Owojori, Foliar application of zinc alleviates the heat stress of pakchoi (*Brassica chinensis* L.). *J. Plant Nutr.* **43**, 194–213 (2020).
51. T. Masuda, Recent overview of the Mg branch of the tetrapyrrole biosynthesis leading to chlorophylls. *Photosynth. Res.* **96**, 121–143 (2008).
52. J. Amaral, A. K. M. Lobo, E. Carmo-Silva, Regulation of Rubisco activity in crops. *New Phytol.* **241**, 35–51 (2024).
53. I. Yruela, Transition metals in plant photosynthesis. *Metalomics* **5**, 1090–1109 (2013).
54. M. A. Gururani, J. Venkatesh, L. S. P. Tran, Regulation of photosynthesis during abiotic stress-induced photoinhibition. *Mol. Plant* **8**, 1304–1320 (2015).
55. M. Asgher *et al.*, Hydrogen peroxide modulates activity and expression of antioxidant enzymes and protects photosynthetic activity from arsenic damage in rice (*Oryza sativa* L.). *J. Hazard. Mater.* **401**, 123365 (2021).
56. X. Cao *et al.*, Lanthanum silicate nanomaterials enhance sheath blight resistance in rice: Mechanisms of action and soil health evaluation. *ACS Nano* **17**, 15821–15835 (2023).
57. J. Joun, R. Sirohi, S. J. Sim, The effects of acetate and glucose on carbon fixation and carbon utilization in mixotrophy of *Haematococcus pluvialis*. *Bioresour. Technol.* **367**, 128218 (2023).
58. M.-H. Liang *et al.*, Orange protein (DbBOR) from the salt-tolerant green alga *Dunaliella bardawil* mediates photosynthesis against heat stress via interacting with DbPsbP1. *Algal Res.* **72**, 103105 (2023).
59. J. Sacharz, V. Giovagnetti, P. Ungerer, G. Mastrianni, A. V. Ruban, The xanthophyll cycle affects reversible interactions between PsbS and light-harvesting complex II to control non-photochemical quenching. *Nat. Plants* **3**, 16225 (2017).
60. T. Chen *et al.*, A plant genetic network for preventing dysbiosis in the phyllosphere. *Nature* **580**, 653–657 (2020).
61. A. Mukherjee *et al.*, Harnessing of phytomicrobiome for developing potential biostimulant consortium for enhancing the productivity of chickpea and soil health under sustainable agriculture. *Sci. Total Environ.* **836**, 155550 (2022).
62. Y. Chi *et al.*, Plant growth promoting endophyte promotes cadmium accumulation in *Solanum nigrum* L. by regulating plant homeostasis. *J. Hazard. Mater.* **457**, 131866 (2023).
63. C. Gao *et al.*, Co-occurrence networks reveal more complexity than community composition in resistance and resilience of microbial communities. *Nat. Commun.* **13**, 3867 (2022).
64. M. M. Yuan *et al.*, Climate warming enhances microbial network complexity and stability. *Nat. Clim. Change* **11**, 343–348 (2021).
65. N. Xu *et al.*, Phyllosphere microorganisms: Sources, drivers, and their interactions with plant hosts. *J. Agr. Food Chem.* **70**, 4860–4870 (2022).
66. R. R. Junker, D. Tholl, Volatile organic compound mediated interactions at the plant-microbe interface. *J. Chem. Ecol.* **39**, 810–825 (2013).
67. M. Guo *et al.*, Response of microbial communities in the tobacco phyllosphere under the stress of valiadimycin. *Front. Microbiol.* **14**, 1328179 (2024).
68. M. O. Adomako, F.-H. Yu, Potential effects of micro- and nanoplastics on phyllosphere microorganisms and their evolutionary and ecological responses. *Sci. Total Environ.* **884**, 163760 (2023).
69. H. J. De Boeck, F. E. Dreesen, I. A. Janssens, I. Nijs, Climatic characteristics of heat waves and their simulation in plant experiments. *Global. Change Biol.* **16**, 1992–2000 (2010).
70. S. V. K. Jagadish, P. Q. Craufurd, T. R. Wheeler, High temperature stress and spikelet fertility in rice (*Oryza sativa* L.). *J. Exp. Bot.* **58**, 1627–1635 (2007).
71. S. Guo, X. Hu, F. Yu, L. Mu, Heat waves coupled with nanoparticles induce yield and nutritional losses in rice by regulating stomatal closure. *ACS Nano* **18**, 14276–14289 (2024).
72. S. Laughlin *et al.*, Methanol-based extraction protocol for insoluble and moderately water-soluble nanoparticles in plants to enable characterization by single particle ICP-MS. *Anal. Bioanal. Chem.* **413**, 299–314 (2021).
73. J.-H. Shi *et al.*, Nitrogen and growth stage influence epicuticular wax composition on rice leaf and sheath. *ACS Agric. Sci. Technol.* **3**, 413–420 (2023).
74. S. Guo *et al.*, Zinc oxide nanoparticles cooperate with the phyllosphere to promote grain yield and nutritional quality of rice under heatwave stress. Baidu Netdisk. [https://pan.baidu.com/s/1pMcrc\\_pxygfMOMgNQqQiAw?pwd=3q3q](https://pan.baidu.com/s/1pMcrc_pxygfMOMgNQqQiAw?pwd=3q3q). Deposited 19 October 2024.